Sains Malaysiana 53(11)(2024): 3709-3719
http://doi.org/10.17576/jsm-2024-5311-14

Synthesis and Characterization of Poly (Ethylene Glycol) Dimethacrylate-Based Bionanocomposites with Hydroxyapatite from Rohu Fish (*Labeo rohita*) Bones

(Sintesis dan Pencirian Bionanokomposit Berasaskan Poli (Etilena Glikol) Dimetakrilat dengan Hidroksiapatit daripada Tulang Ikan Rohu (*Labeo rohita*))

BUSHRA INAM[1], NARGIS JAMILA[2], NAEEM KHAN[1], SAEED AHMAD KHAN[3], UMAR NISHAN[1], ALEESHA RAUF[1], SHAUKAT SHUJAH[1], AZHAR UL HAQ ALI SHAH[1], MOHAMED A. IBRAHIM[4] & KYONG SU KIM[5,*]

[1]*Department of Chemistry, Kohat University of Science and Technology, Kohat 26000, Khyber Pakhtunkhwa, Pakistan*
[2]*Department of Chemistry, Shaheed Benazir Bhutto Women University, Peshawar 25000, Khyber Pakhtunkhwa, Pakistan*
[3]*Department of pharmacy, Kohat University of Science and Technology, Kohat 26000, Khyber Pakhtunkhwa, Pakistan*
[4]*Department of Pharmaceutics, College of Pharmacy, King Saud University, Riyadh 11451, Saudi Arabia*
[5]*Department of Food and Nutrition, Chosun University, Gwangju 61452, Republic of Korea*

Received: 15 August 2024/Accepted: 18 September 2024

ABSTRACT

Hydroxyapatite (HA) has gained significant recognition as a bioceramic with widespread utilization in diverse biomedical fields such orthopedics and dentistry. The present study was aimed to isolate hydroxyapatite from rohu fish bones and integrate it into biomaterials with the potential for use in dentistry. Nanocomposite films were developed by combining hydroxyapatite and irgacure with poly (ethylene glycol) dimethacrylate (PEGDMA) and characterized by SEM, DSC, FTIR spectroscopy, and XRD techniques. The SEM study identified HA as nanospheres with crystal sizes below 30 nm. When incorporated into PEGDMA, these nanoparticles aggregated, potentially disrupting polymer chain interactions and affecting the films' mechanical properties. The XRD pattern obtained from the fish bone subjected to higher temperature calcination exhibited highly intense and sharp peaks, indicating the removal of the organic portion. The FTIR results confirmed the disappearance of carbon-to-carbon double bonds due to the successful free radical polymerization reaction. The high enthalpy of fusion for PEGDMA and irgacure 2952 (86.1409 kJ/mol) suggested that they required high energy to melt, while their exothermic crystallization enthalpy (21.35378 kJ/mol) indicated the heat release upon solidification. Adding hydroxyapatite reduced these enthalpies, indicating easier melting and solidification, which may aid processing thus opens new possibilities for biomedical applications, particularly in dentistry.

Keywords: Hydroxyapatite (HA); irgacure; poly (ethylene glycol) dimethacrylate (PEGDMA); rohu fish (*Labeo rohita*) bones

ABSTRAK

Hidroksiapatit (HA) telah mendapat pengiktirafan yang ketara sebagai bioseramik dengan penggunaan meluas dalam pelbagai bidang bioperubatan seperti ortopedik dan pergigian. Kajian ini bertujuan untuk mengasingkan hidroksiapatit daripada tulang ikan rohu dan mengintegrasikannya ke dalam biobahan yang berpotensi untuk digunakan dalam pergigian. Filem nanokomposit telah dibangunkan dengan menggabungkan hidroksiapatit dan irgacur dengan poli (etilena glikol) dimetakrilat (PEGDMA) dan dicirikan oleh teknik SEM, DSC, FTIR dan XRD. Kajian SEM mengenal pasti HA sebagai nanosfera dengan saiz kristal di bawah 30 nm. Apabila digabungkan ke dalam PEGDMA, zarah nano ini terkumpul, berpotensi mengganggu interaksi rantai polimer dan menjejaskan sifat mekanikal filem. Corak XRD yang diperoleh daripada tulang ikan yang tertakluk kepada pengkalsinan suhu yang lebih tinggi menunjukkan puncak yang sangat sengit dan tajam, menunjukkan penyingkiran bahagian organik. Keputusan FTIR mengesahkan kehilangan ikatan berganda karbon-ke-karbon kerana tindak balas pempolimeran radikal bebas yang berjaya. Entalpi pelakuran yang tinggi untuk PEGDMA dan irgacur 2952 (86.1409 kJ/mol) mencadangkan bahawa ia memerlukan tenaga yang tinggi untuk mencairkan, manakala entalpi penghabluran eksotermiknya (21.35378 kJ/mol) menunjukkan pelepasan haba apabila pemejalan. Menambah hidroksiapatit mengurangkan entalpi ini, menunjukkan pencairan dan pemejalan yang lebih mudah, yang boleh membantu pemprosesan sekali gus membuka kemungkinan baharu untuk aplikasi bioperubatan, terutamanya dalam pergigian.

Kata kunci: Hidroksiapatit (HA); irgacur; poli (etilena glikol) dimetakrilat (PEGDMA); tulang ikan rohu (*Labeo rohita*)

INTRODUCTION

Hydroxyapatite (HA) is becoming one of the most important bioceramic, which is widely used in various biomedical applications, mainly in orthopedics and dentistry due to close similarities with inorganic mineral content of bone and teeth. Naturally occurring hydroxyapatite is hexagonal in structure with the chemical formula of one-unit cell being $Ca_{10}(PO_4)_6(OH)_2$, possesses exceptional biocompatibility and unique bioactivity (Nayak 2010). HA is a calcium phosphate-based bioceramic, which has been used in medicine and dentistry for over 20 years due to its excellent biocompatibility with human tissue (Hench 1998). Consequently, HA has found extensive application in the field of dental implants (Soballe & Overgaard 1996). Extensive research has been conducted on this material for use in orthopedic and dental implants, and the findings have consistently demonstrated its exceptional bioactivity, sufficient mechanical strength and structure, ability to promote bone growth, support for blood vessel formation, lack of toxicity, and absence of inflammatory or immune responses (Appleford et al. 2009). It is widely recognized that bone tissue forms a direct bond with hydroxyapatite (HA) through the presence of a carbonated, calcium-deficient apatite layer at the interface between the bone and the implant. This interaction stimulates the deposition of newly generated bone following the implantation procedure (Kattimani et al. 2016). In recent years, hydroxyapatite (HA) derived from fish bones and scales has gained importance as a viable alternative to replace synthetic and bovine-derived HA. This shift is due to the successful attainment of comparable chemical properties through straightforward and cost-effective methods. Researchers have confirmed that fish-derived sources are safe and involve minimal risks associated with disease transmission (Hoyer et al. 2012). Moreover, fish are abundant in the environment, and using their byproducts in biomedical applications is eco-friendly, as it helps to reduce environmental pollution and lowers potential biohazards to humans (Venkatesan et al. 2012).

A variety of fish species, including but not limited to salmon, carp, Japanese anchovy, sardine, tilefish, and tuna have been utilized to acquire HA. To achieve this, numerous extraction protocols and chemical analysis methods have been suggested in literature, all with the common objective of obtaining and characterizing HA extracted from fish sources (Hamada et al. 1995). PEGDMA, short for poly (ethylene glycol) dimethacrylate, is a monomer belonging to the family of poly (ethylene glycol) (PEG) derivatives. It holds extensive applications in dentistry and polymer chemistry. This monomer is formed by the reaction of poly (ethylene glycol) with either methacrylic acid or methacrylic anhydride. Consequently, the resulting compound contains multiple methacrylate functional groups and poly (ethylene glycol) chains. The molecular weight and properties of PEGDMA can differ based on the number of repeating ethylene glycol units (Ilagan & Amsden 2009). PEGDMA is widely recognized for its use in dental materials, particularly in dental composites and adhesives. Its primary function lies in acting as a crosslinking agent that binds together the different monomers present in the composite or adhesive formulation. Through this crosslinking process, dental materials gain enhanced mechanical strength and stability (Sania et al. 2012). The inclusion of poly (ethylene glycol) chains in PEGDMA imparts several beneficial properties to the resulting dental materials. It enhances the water solubility of the material, making it more manageable during placement. PEGDMA also effectively reduces polymerization shrinkage, a common issue in dental composites that can lead to marginal gaps and sensitivity. Moreover, the presence of PEGDMA contributes to the overall enhancement of biocompatibility in dental materials (Kumar et al. 2016). The bonding between HA particles and the polymer matrix significantly impacted the properties of HA/polymer composites, being one of the key factors. To enhance the interfacial strength between the two phases, several techniques have been employed. For instance, Qiu et al. (2005) utilized ring-opening polymerization of L-lactide on HA surfaces along with the esterification of poly-L-lactic acid (PLLA) and HA and hydroxyapatite nanoparticles were evenly distributed within the PLLA matrix and demonstrated enhanced adhesion to it. As a result, the HA-g-PLLA/PLLA composites possessed superior mechanical properties compared to the basic n-HA/PLLA blends. According to Liu et al. (1998), isocyanate was employed to react with hydroxyl groups on the HA surface to make poly (ethylene glycol) (PEG)/HA and poly (methyl methacrylate) (PMMA)/HA composites by modifying the HA surface with diisocyanate and polymer. Pramanik et al. (2009) found that the symphonic acid group in 2-carboxyethyl symphonic acid could firmly attach to the apatite surface, while the reactive carboxyl terminal increased chemical interactions with the polymer's hydroxyl groups. This resulted in improved interfacial bonding between HA nanoparticles and the poly (ethylene-co-vinyl alcohol) matrix. In another study, HA nanoparticles were synthesized *in situ* within poly (ethylene glycol) dimethacrylate (PEGDMA). These composites demonstrated superior dispersion of the inorganic phase and enhanced mechanical properties compared to those formed by physically mixing HA with PEGDMA (Zhou et al. 2009). PEGDMA is an unsaturated linear polyether, characterized by a polyethylene glycol main chain and methacrylate end groups, which can be photocrosslinked *in situ* (Lin-Gibson et al. 2004). In bone tissue engineering, PEG, which forms the main chain of PEGDMA, can reduce protein adsorption and cell adhesion on the surface of bone substitutes, thereby, enhancing bone remodeling (Yang et al. 2005). A

photo initiator, also referred as a chemical compound that triggers a photochemical reaction when exposed to light. It is commonly employed in various industries like printing, coatings, adhesives, and 3D printing to initiate or speed up the curing or polymerization process. An illustrative instance is the Irgacure® 2959, an exceptionally efficient radical photoinitiator that finds application in UV curing systems (Ge, Trujillo & Stansbury 2005).

In the current study, poly (ethylene glycol) dimethacrylate (PEGDMA) was used for cross linking with HA, synthesized from an unexplored source of rohu fish (*Labeo rohita*) bones for possible tooth structure remineralization applications. Two categories of films were developed: The first category was irgacure fabricated in PEGDMA, having no HA, while the second category incorporated HA nanoparticles along with irgacure in PEGDMA. UV light exposure induced the formation of crosslinked gels. These gels, with PEGDMA serving as a binding matrix, were found to be biocompatible, and capable of forming stable networks.

MATERIALS AND METHODS

MATERIALS

Poly (ethylene glycol) dimethacrylate of analytical grade having molecular weight 550 g/mol was obtained from Sigma Aldrich, (USA). Irgacure 2959, was purchased from Sigma Aldrich, (USA). Hydroxyapatite nanoparticles (HA) were synthesized in the research lab.

SYNTHESIS OF HYDROXYAPATITE FROM ROHU FISH BONES

To perform the alkaline hydrolysis procedure, rohu fish (*Labeo rohita*) bones were boiled for 15 min to completely remove any remaining meat. Subsequently, the fish bones were treated with sodium hydroxide (NaOH) at 250 °C for 5 h to eliminate organic components. The resulting mixture was filtered using a suction pump and washed continuously with water until a neutral pH was achieved. The materials were then dried in an oven at 100 °C. For the thermal calcination process, the dried fish bones were placed in a silica crucible and heated to 900 °C in a muffle furnace, as depicted in Figure 1.

SYNTHESIS OF BIONANOCOMPOSITES BY CROSSLINKING

Two categories of films were generated: The first consisted of blank films without hydroxyapatite, while the second comprised films loaded with hydroxyapatite. For the blank film preparation, irgacure was introduced into poly (ethylene glycol) dimethacrylate (PEGDMA 550). Simultaneously, an additional film was developed by incorporating irgacure into PEGDMA along with hydroxyapatite nanoparticles. This film was then exposed to ultraviolet light for 3 h. Crosslinked gels were formed and allowed to solidify completely at ambient temperature for a period of 2 h. Following this, the resultant gels were subjected to washing with distilled water, as shown in Figure 2. The PEGDMA component within the nanocomposites functioned as a binding matrix, effectively holding together the hydroxyapatite nanoparticles. PEGDMA attributes, include its favorable biocompatibility, low toxicity, and capacity to make stable crosslinked networks as shown in Figure 3.

CHARACTERIZATION OF SYNTHESIZED BIONANOCOMPOSITES

The qualitative structure of the hydroxyapatite nanoparticles was analyzed by FTIR spectroscopic measurements (Perkin Elmer, Spectrum 100 model, Waltham, MA, USA). The instrument was operated in transmission mode with a resolution of 1 cm^{-1} and covered a wavelength range of 450-4000 cm^{-1}. To analyze the samples, small pieces were prepared and placed in a palette holder, which was then mounted in the FTIR instrument, and all spectra were recorded at room temperature. The X-ray diffraction (JDX-3532, JEOL, Japan) analysis patterns of hydroxyapatite and nanocomposites were recorded at room temperature on 2theta-range (0 to 160°) with CuKα λ (1.5418 Å) radiations. The current and operating voltage were 2.5-30 mA, and 20-40 kV. The morphology of hydroxyapatite nanoparticles and PEGDMA/HA nanocomposites was determined using SEM (Jeol, JSM-5910 LV, Japan). It was operated at an energy level of 30 kV, allowing for detailed imaging and analysis of samples. The maximum achievable magnification was 300,000 times, enabling the examination of fine structural features. Additionally, the SEM exhibited a maximum resolving power of 2.3 nm, ensuring high-resolution imaging and the ability to distinguish fine details in the samples. Differential scanning calorimetry (Perkin-Elmer USA) was utilized to determine the heat of reaction of each sample. About 10-12 mg of samples were placed in DSC aluminum pans, hermetically sealed, and then transferred to the instrument's sample holder. The curing experiments were conducted under nitrogen at heating rates ranging from 20 to 50 °C/min.

RESULTS AND DISCUSSION

The FTIR spectra (as shown in Figure 4(a)) showed distinct peaks related to the OH group at 3511 cm^{-1}, the phosphate group at 500 to 1100 cm^{-1}, and carbonate group at 1459 cm^{-1} (Figure 4(a)). From the results of alkaline hydrolysis

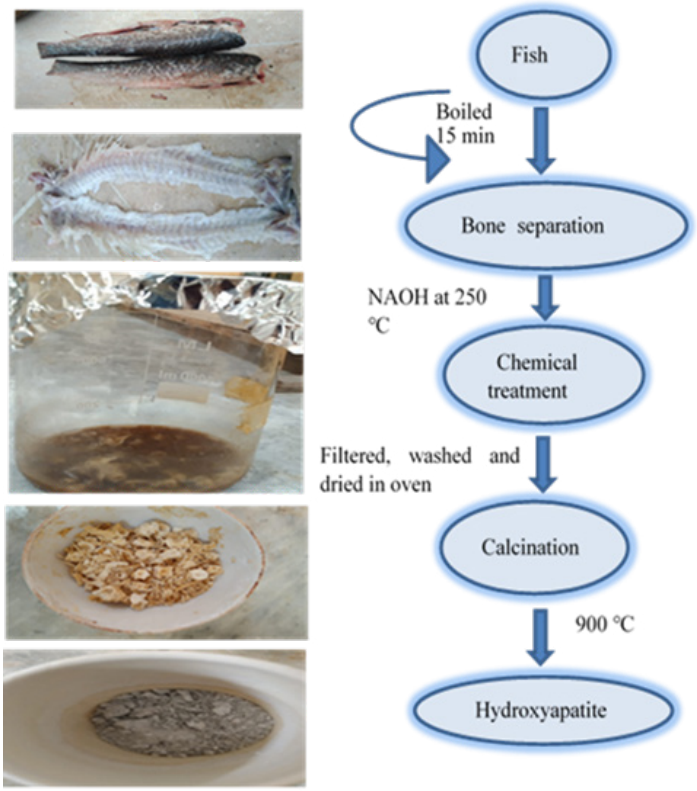

FIGURE 1. Synthesis of hydroxyapatite (HA) from rohu fish bones

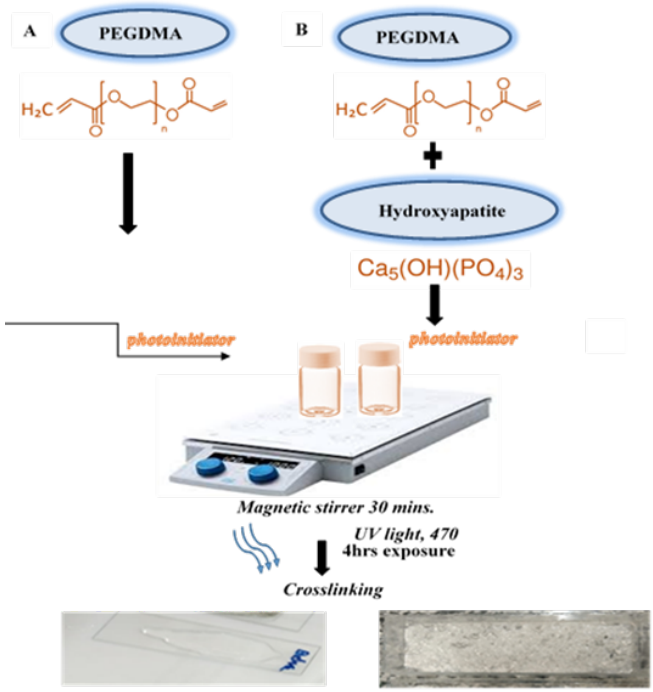

FIGURE 2. Synthesis of HA/PEGDMA bionanocomposite films

and thermal calcination techniques as shown in Table 1, it was deduced that the organic portion was eliminated, thus, confirming the existence of carbonated HA crystals. The FTIR analysis showed that the chemical compositions of films containing HA did not exhibit any new peaks. This is because most of the HA peaks were overlapping with those of PEGDMA, and there were no significant shifts in peaks when HA was added. Therefore, it can be concluded that the addition of HA did not significantly alter the chemical composition of the PEGDMA-based hydrogel as shown in Figure 4(b). The FT-IR analysis of the PEGDMA component gave important information about crosslinking and shape changes in the nanocomposite. Significant changes, like shifts or changes in intensity in the C=C double bond region, and the appearance of new bands, suggested that crosslinking reactions might have happened within the PEGDMA molecules (Arslan et al. 2022). These changes can significantly affect the overall strength and stability of the nanocomposite structure (Maleki et al. 2022). Additionally, the changes observed in the FT-IR spectrum of PEGDMA in the nanocomposite also suggested alterations in the polymer's shape or flexibility, possibly due to the interactions with the hydroxyapatite component (Raguraman & Rajan 2023). The noticeable shifts and broadening of peaks related to the O-H stretching vibrations strongly indicated the formation of hydrogen bonds between the hydroxyapatite (HA) and poly (ethylene glycol) dimethacrylate (PEGDMA) components. This establishment of hydrogen bonds plays a crucial role in strengthening the overall stability and cohesiveness of the nanocomposite structure, thereby potentially enhancing its mechanical properties (Jin et al. 2022). This observation aligns with prior reported research, which has indicated that hydrogen bonding enhances the mechanical properties of polymer-ceramic composite system (Huang et al. 2022).

X-ray diffraction (XRD) is a reliable, non-destructive method for assessing the phase purity and crystallinity of materials (Moureen et al. 2024). In this study, XRD was used to confirm the phase and purity of hydroxyapatite (HA) crystals. Three samples were analyzed including untreated bone, HA synthesized through alkaline hydrolysis, and HA derived from thermal calcination. According to Pupilli et al. (2022), the untreated bone exhibited broad reflections, suggesting biologically mineralized, low-crystalline HA mixed with organic material. However, the thermally calcined bone displayed sharp, well-defined peaks indicative of organic component removal and a higher crystallinity level. The alkaline hydrolyzed bone showed less distinct peaks compared to the calcined sample, indicating a lower degree of crystallinity. The XRD pattern from the fish bone subjected to high-temperature calcination showed intense and sharp peaks, indicating that the organic material was effectively removed (Jamila et al. 2021). This implies that the hydroxyapatite (HA) in the bone remained stable during calcination up to 900 °C, with no other peaks detected besides those of HA. Key parameters in the XRD analysis of HA included peak shape, position, width, and intensity, which were critical for its characterization (Figure 5(a)) (Table 2). The XRD pattern exhibited distinct peaks at 2θ angles around 25.8°, 31.8°, 32.2°, 32.9°, 34.0°, and 39.8°, corresponding to the (002), (211), (112), (300), (202), and (310) crystallographic planes of hydroxyapatite, respectively. These characteristic peaks strongly indicated the formation of hydroxyapatite as the main crystallographic phase. Using the Scherrer equation to analyze the (002) peak, the estimated average crystallite size of the hydroxyapatite sample was found to be between 20 and 30 nm, which was consistent as reported in literature for nanocrystalline hydroxyapatite produced (Venkatesan et al. 2011). By comparing the XRD pattern, the obtained standards listed in the Joint Committee on Powder

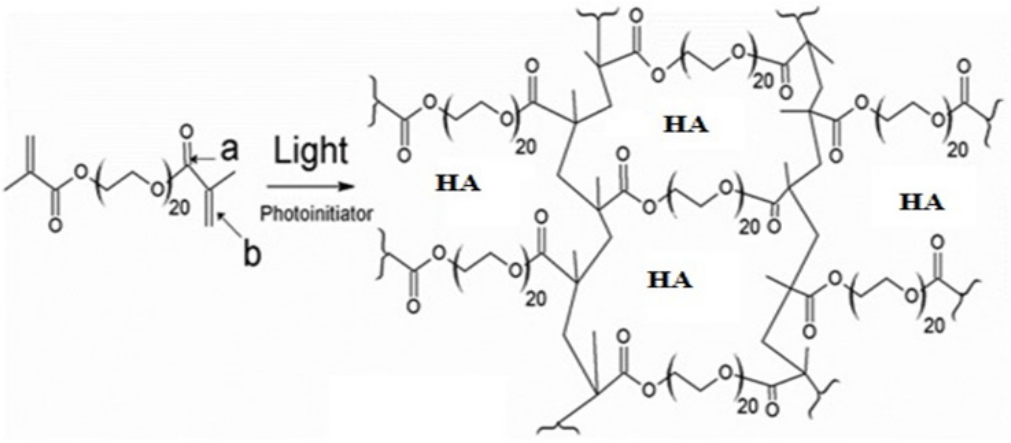

FIGURE 3. Photo crosslinked HA/PEGDMA bionanocomposite polymer

TABLE 1. Assignment of the FTIR spectra of hydroxyapatite from rohu fish bones

Methods	IR absorption bands (cm^{-1})	Description
Thermal calcination	1050, 1089	$\nu3(PO_4^{3-})$
	962	$\nu1(PO_4^{3-})$
	571	$\nu4(PO_4^{3-})$
	1415, 1459	$\nu3(CO_3^{2-})$
	634	Bending OH^-
Alkaline hydrolysis	1044, 1099	$\nu3(PO_4^{3-})$
	963	$\nu1(PO_4^{3-})$
	566	$\nu4(PO_4^{3-})$
	1417, 1455	$\nu3(CO_3^{2-})$
	875	$\nu2(CO_3^{2-})$
	632	Bending OH^-
	3568	$\nu(OH)$

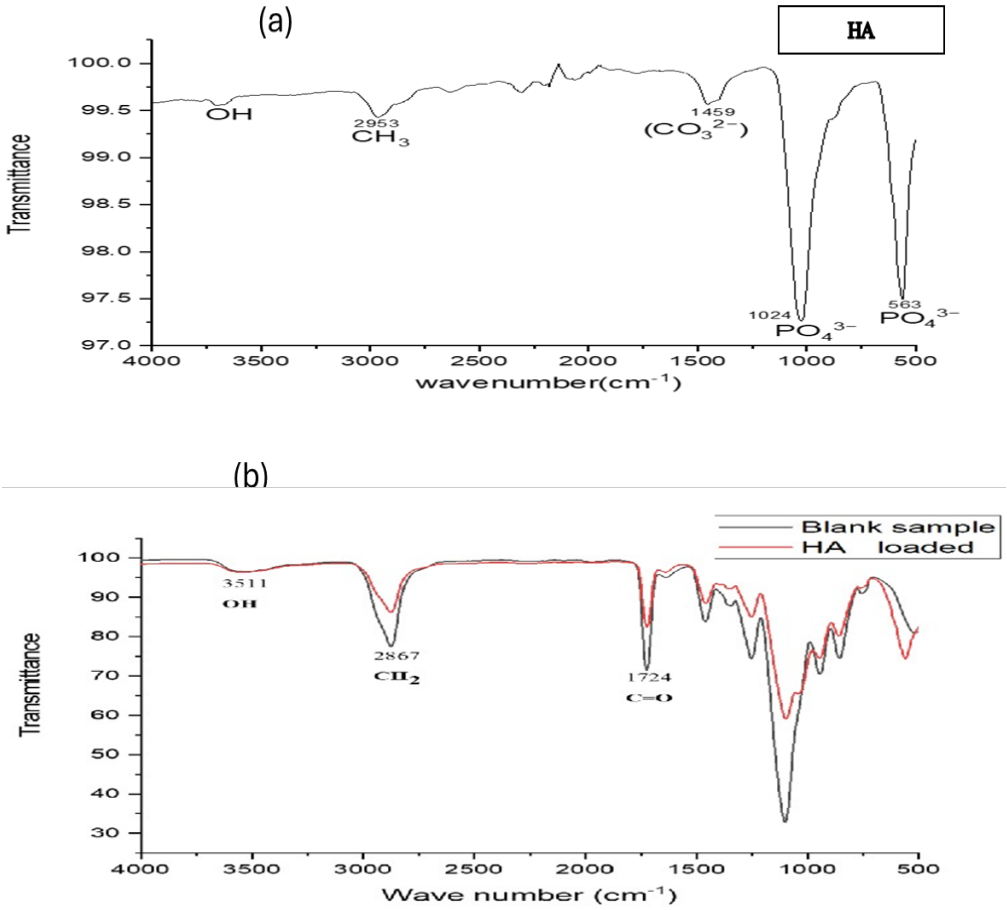

FIGURE 4. FT-IR spectra of pure hydroxyapatite, blank sample and blank sample loaded with hydroxyapatite, (a) FT-IR spectra of pure hydroxyapatite, (b) FT-IR spectra of blank sample and hydroxyapatite loaded sample

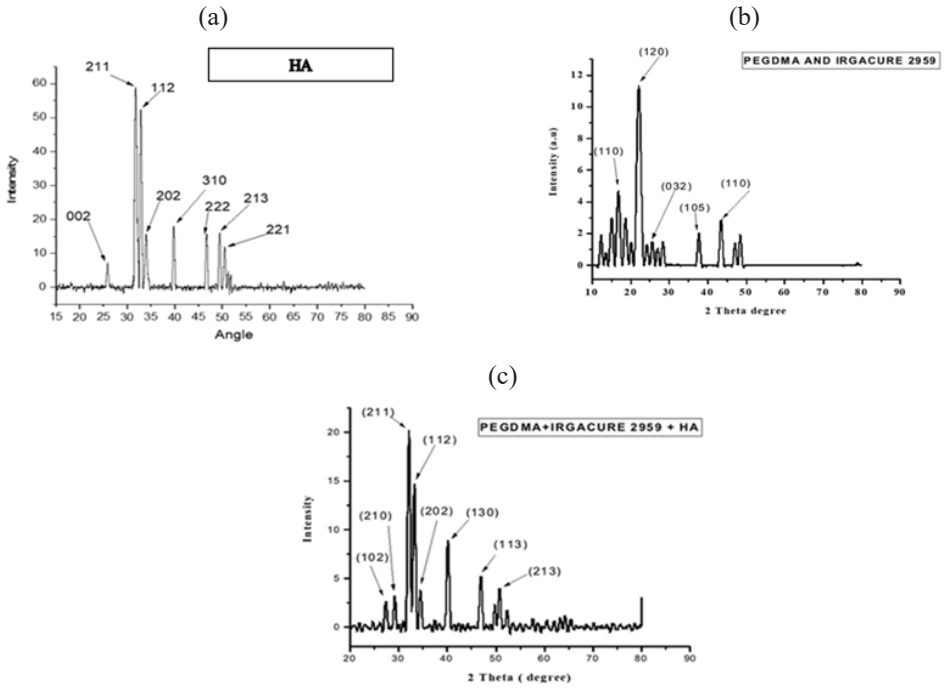

FIGURE 5. XRD pattern of hydroxyapatite, blank sample and hydroxyapatite loaded sample, (a) XRD pattern of hydroxyapatite, (b) XRD pattern of blank sample, (c) XRD pattern of hydroxyapatite loaded sample

TABLE 2. XRD data of standard hydroxyapatite JCPDS-090432—HA

Crystallographic plane (h k l)	Angle (θ)	d-Spacing (nm)	Intensity (%)
0 0 2	25.879	0.3440	40
2 1 1	31.774	0.2814	100
1 1 2	32.197	0.2778	60
3 0 0	32.902	0.2720	60
2 0 2	34.049	0.2631	25
3 1 0	39.819	0.2261	20
2 2 2	46.713	0.1943	30
2 1 3	49.469	0.1841	40
3 2 1	50.494	0.1806	20
0 0 4	53.145	0.1722	20

TABLE 3. XRD data of blank sample without hydroxyapatite

Crystallographic plane (h k l)	Angle (θ)	d-Spacing (nm)	FWHM
1 1 0	18.4	4.3	0.96
1 2 0	22.4	4.02	0.83
0 3 2	25.3	4.02	0.83
1 0 5	36.5	2.4	1.15
1 1 0	44.4	2.08	1.15

TABLE 4. XRD data of hydroxyapatite loaded sample

Crystallographic Plane (h k l)	Angle (θ)	d-Spacing (nm)	FWHM
1 0 2	28.1	3.40	0.787
2 1 0	30.3	3.08	0.31
2 1 1	33.2	2.79	0.078
1 1 2	35.2	2.6	0.393
2 0 2	36.8	2.6	0.393
1 3 0	41.1	2.24	0.196
1 1 3	48.3	1.93	0.236
2 1 3	51.3	1.33	0.236

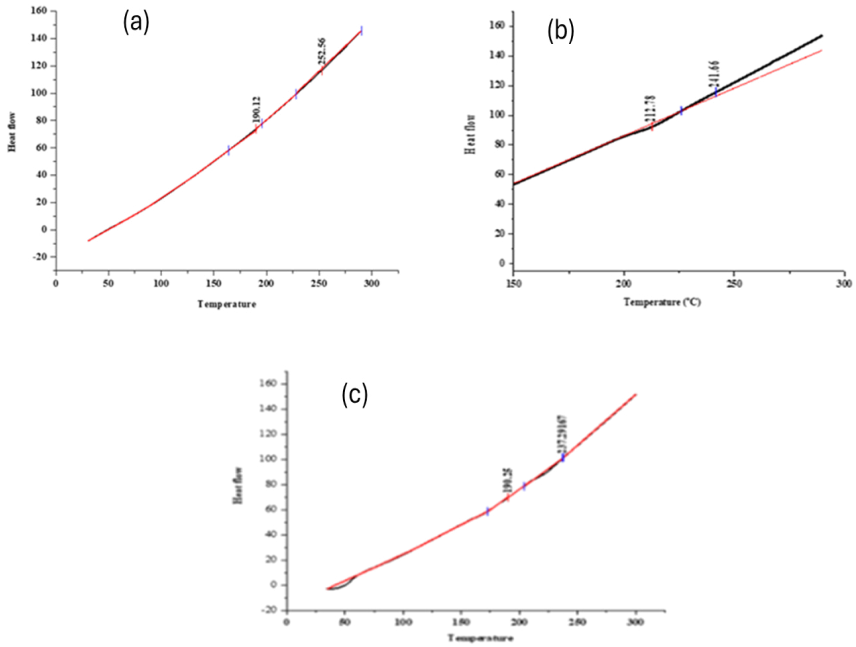

FIGURE 6. DSC graphs of pure hydroxyapatite, blank sample and hydroxyapatite loaded sample, (a) DSC graph of pure hydroxyapatite, (b) DSC graph of blank sample, and (c) DSC graph of hydroxyapatite loaded sample

TABLE 5. Data of blank sample, hydroxyapatite loaded sample and pure hydroxyapatite

Parameter	Enthalpy of fusion	Enthalpy of crystallization
Blank sample	86.1409	21.35378
HA loaded	3.54094	0.00189
Pure HA	66.23	25.121

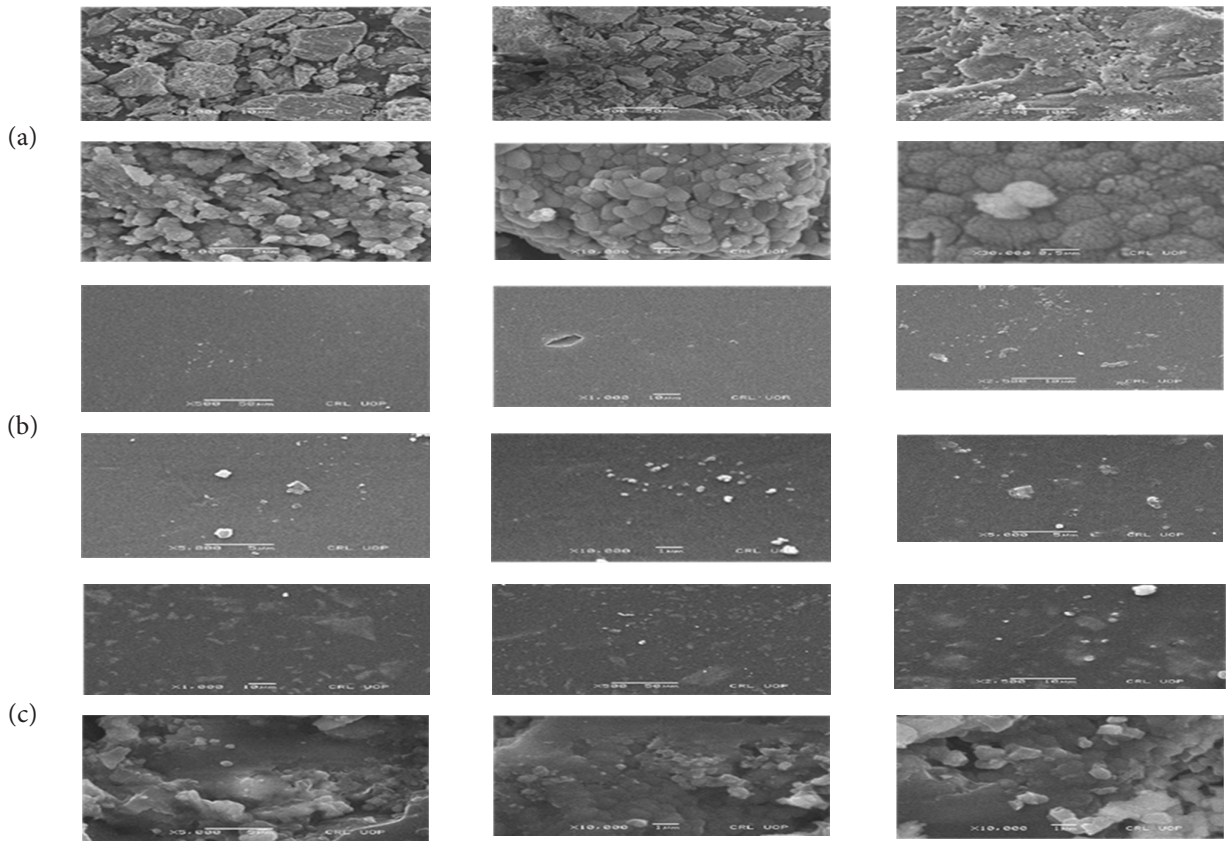

FIGURE 7. SEM micrographs pure hydroxyapatite, blank sample and hydroxyapatite loaded sample, (a) SEM micrograph of pure hydroxyapatite, (b) SEM micrograph of blank sample, (c) SEM micrograph of hydroxyapatite loaded sample

Diffraction Standards (JCPDS) database, can be applied for a qualitative analysis. As the temperature increases, the intensity of the peaks usually rises, and the peaks become narrower. Table 2 shows the high-intensity peak of reference hydroxyapatite (HA) from the JCPDS (Barakat et al. 2023). While Barakat et al. (2023) have reported in literature that the thermal calcination method led to the near-complete removal of the carbonate group from bovine bone, our investigation unveiled a differing outcome. Specifically, when subjecting fish bone to elevated temperatures (900 °C for 5 h), the carbonate group was found to be retained rather than eliminated (Brahimi et al. 2022). In the x-ray diffraction analysis of the prepared blank sample (Figure 5(b)), five prominent peaks were observed at precise 2θ values: 15.18°, 23.24°, 25.22°, 34.38°, and 42.45°, corresponding to specific Miller indices (110), (120), (032), (105), and (110) (Table 3). The analysis also showed that the average crystallite size of the blank sample measured approximately 12 nm. The observed peak positions, d-spacing values, and peak intensities collectively signify the unequivocal crystalline nature of the synthesized films. Specifically, the presence of these peaks aligns with the expected characteristics of an orthorhombic crystal structure. Moreover, these findings support the assertion that the synthesized material demonstrates orthorhombic properties, substantiating the XRD analysis results.

Similarly, the XRD pattern of HA-loaded samples exhibited a broad band from 2θ = 26.2° to 50.3° (Figure 5(c)). The peak positions, d-spacing, intensities, and the average crystallite size of HA-loaded samples (13 nm) suggested the crystalline nature of the synthesized films, with orthorhombic characteristics, also indicated by the primitive factor (Table 4). This suggested that the existence of HA crystals might disrupt the arrangement of PEGDMA-based polymer chains, leading to diminished crystalline characteristics within the composite scaffolds.

Figure 6(a)-6(c), display DSC curves for HA, PEGDMA, and HA/PEGDMA films, respectively, showed distinct melting points and glass transition temperatures. Notably, the enthalpy of fusion (86.1409 kJ/mol) for PEGDMA and Irgacure 2952, along with the exothermic enthalpy of crystallization (21.35378 kJ/mol), highlights their energy

requirements for melting and solidification, crucial for material stability and processing. The incorporation of hydroxyapatite results in reduced enthalpies of fusion (3.54094 kJ/mol) and crystallization (0.00189 kJ/mol), suggesting easier melting and solidification, potentially aiding material processing. For hydroxyapatite, the enthalpy of fusion (66.23 kJ/mol) signified the energy needed for its melting, while the enthalpy of crystallization (25.121 kJ/mol) denoted the heat release upon solidification, both are important for applications such as dental materials.

This DSC analysis explained material behavior and suitability for specific applications. The morphological examination of hydroxyapatite nanoparticles was conducted using a scanning electron microscope (SEM). The hydroxyapatite nanoparticles exhibited significant agglomeration. The structure and morphology of HA depends upon the source and reaction conditions like pH. Therefore, the MP of HA was not so sharp. It is also possible that HA might have started breaking down before it melts, thus preventing a clear melting peak.

The SEM analysis showed spherical particles with clustered distributions, classifying the HA particles as nanospheres with crystal sizes below 30 nm as illustrated in Figure 7(a). Figure 7(b) and 7(c) was taken to investigate the morphology of hydrogels without and with HA. Films lacking HA displayed small, smooth blocks without noticeable surface variation within the SEM observable size range (Khan et al. 2022). The HA particles were added to the PEGDMA networks, causing some aggregation. The clustered HA particles might have interfered with the polymer chains, causing the cross-linked film network to separate. This can affect the mechanical properties and the temperature at which the hydrogel reactions happen.

CONCLUSIONS

The primary aim of this study was to extract pure natural hydroxyapatite (HA) from Rohu fish bones using a combination of alkaline hydrolysis and thermal calcination methods and the successful incorporation of hydroxyapatite (HA) into poly (ethylene glycol) dimethacrylate (PEGDMA)-based films which has led to significant advancements in biocompatibility. The introduction of HA into the films resulted in a remarkable improvement in biocompatibility compared to films without HA. This enhancement opens new possibilities for biomedical applications, particularly in dentistry. The FTIR findings demonstrated that the introduction of HA did not significantly alter the chemical composition of PEGDMA-based films, while SEM and XRD results exhibited changes in morphology which emphasized the compatibility of HA with the existing film structure, reinforcing the stability of the composite material. Additionally, the composite hydrogels of PEGDMA and HA, exhibiting enhanced biocompatibility, hold tremendous potential for applications such as tooth structure remineralization. Beyond its biomedical significance, the study's dual impact in addressing environmental concerns by using Rohu fish bone waste highlights its broader implications. This work lays the foundation for future research and applications, emphasizing the synergy between environmental sustainability and advancements in biomedical materials.

ACKNOWLEDGEMENTS

The authors extend their appreciation to the Researchers Supporting Project (RSP2024R171), King Saud University, Riyadh, Saudi Arabia for financial support. The authors declare that they have no known competing financial interests or personal relationships that could have appeared to influence the work reported in this paper.

REFERENCES

Appleford, M.R., Oh, S., Oh, N. & Ong, J.L. 2009. *In vivo* study on hydroxyapatite scaffolds with trabecular architecture for bone repair. *Journal of Biomedical Materials Research Part A* 89(4): 1019-1027.

Arslan, M.E., Kurt, M.Ş., Aslan, N., Kadi, A., Öner, S., Çobanoğlu, Ş. & Yazici, A. 2022. Structural, biocompatibility, and antibacterial properties of Ge–DLC nanocomposite for biomedical applications. *Journal of Biomedical Materials Research Part B: Applied Biomaterials* 110(7): 1667-1674.

Barakat, N.A., Sayed, Y.T., Irfan, O.M. & Abdelaty, M.M. 2023. Synthesis of TiO_2-incorporated activated carbon as an effective ion electrosorption material. *PLoS ONE* 18(3): 82-86.

Brahimi, S., Ressler, A., Boumchedda, K., Hamidouche, M., Kenzour, A., Djafar, R., Antunović, M., Bauer, L., Hvizdoš, P., & Ivanković, H. 2022. Preparation and characterization of biocomposites based on chitosan and biomimetic hydroxyapatite derived from natural phosphate rocks, *Materials Chemistry and Physics* 276, 125421.

Ge, J., Trujillo, M. & Stansbury, J. 2005. Synthesis and photopolymerization of low shrinkage methacrylate monomers containing bulky substituent groups. *Dental Materials* 21(12): 1163-1169.

Hamada, M., Nagai, T., Kai, N., Tanoue, Y., Mae, H., Hashimoto, M., Miyoshi, K., Kumagai, H. & Saeki, K. 1995. Inorganic constituents of bone of fish. *Fisheries Science* 61(3): 517-520.

Hench, LL. 1998. Biomaterials: A forecast for the future. *Biomaterials* 19(16): 1419-1423.

Hoyer, B., Bernhardt, A., Heinemann, S., Stachel, I., Meyer, M. & Gelinsky, M. 2012. Biomimetically mineralized salmon collagen scaffolds for application in bone tissue engineering. *Biomacromolecules* 13(4): 1059-1066.

Huang, S.M., Liu, S.M., Ko, C.L. & Chen, W.C. 2022. Advances of hydroxyapatite hybrid organic composite used as drug or protein carriers for biomedical applications: A review. *Polymers* 14(5): 976.

Ilagan, B.G. & Amsden, B.G. 2009. Surface modifications of photocrosslinked biodegradable elastomers and their influence on smooth muscle cell adhesion and proliferation. *Acta Biomaterialia* 5(7): 2429-2440.

Jamila, N., Khan, N., Bibi, N., Waqas, M., Khan, S.N., Atlas, A., Amin, F., Khan, F. & Saba, M. 2021. Hg(II) sensing, catalytic, antioxidant, antimicrobial, and anticancer potential of *Garcinia mangostana* and α-mangostin mediated silver nanoparticles. *Chemosphere* 272: 129794.

Jin, L., Jang, G., Lim, H., Zhang, W., Park, S., Jeon, M. & Kim, W. 2022. Improving the ionic conductivity of PEGDMA-based polymer electrolytes by reducing the interfacial resistance for LIBs. *Polymers* 14(17): 3443.

Kattimani, V., Lingamaneni, K.P., Chakravarthi, P.S., Kumar, T.S. & Siddharthan, A. 2016. Eggshell-derived hydroxyapatite: A new era in bone regeneration. *Journal of Craniofacial Surgery* 27(1): 112-117.

Khan, W., Khan, N., Jamila, N., Masood, R., Minhaz, M., Amin, F., Atlas, A. & Nishan, U. 2022. Antioxidant, antibacterial, and catalytic performance of biosynthesized silver nanoparticles of *Rhus javanica*, *Rumex hastatus*, and *Callistemon viminalis*. *Saudi Journal of Biological Sciences* 29(2): 894-904.

Kumar, A., Tekriwal, S., Rajkumar, B., Gupta, V. & Rastogi, R. 2016. A review on fibre reinforced composite resins. *IP Annals of Prosthodontics and Restorative Dentistry* 2(1): 11-16.

Lin-Gibson, S., Bencherif, S., Cooper, J.A., Wetzel, S.J., Antonucci, J.M., Vogel, B.M. & Washburn, N.R. 2004. Synthesis and characterization of PEG dimethacrylates and their hydrogels. *Biomacromolecules* 5(4): 1280-1287.

Liu, Q., de Wijn, J.R., de Groot, K. & van Blitterswijk, C.A. 1998. Biomaterials, surface modification of nano-apatite by grafting organic polymer. *Biomaterials* 19(11-12): 1067-1072.

Maleki, M., Ghomi, N., Nikfarjam, M., Akbari, E., Sharifi, M.A. & Shahbazi, Y. 2022. Biomedical applications of MXene-integrated composites: Regenerative medicine, infection therapy, cancer treatment, and biosensing. *Advanced Functional Materials* 32(34): 2203430.

Moureen, A., Waqas, M., Khan, N., Jabeen, J., Magazzino, C., Jamila, N. & Beyazli, D. 2024. Untapped potential of food waste derived biochar for the removal of heavy metals from wastewater. *Chemosphere* 356: 141932.

Nayak, A.K. 2010. Hydroxyapatite synthesis methodologies: An overview. *International Journal of ChemTech Research* 2(2): 903-907.

Pramanik, N., Mohapatra, S., Bhargava, P. & Pramanik, P. 2009. Chemical synthesis and characterization of hydroxyapatite (HAp)-poly (ethylene co vinyl alcohol)(EVA) nanocomposite using a symphonic acid coupling agent for orthopedic applications. *Materials Science and Engineering: C* 29(1): 228-236.

Pupilli, F., Ruffini, A., Dapporto, M., Tavoni, M., Tampieri, A. & Sprio, S. 2022. Design strategies and biomimetic approaches for calcium phosphate scaffolds in bone tissue regeneration. *Biomimetics* 7(3): 112.

Qiu, X., Chen, L., Hu, J., Sun, J., Hong, Z., Liu, A. & Jing, X. 2005. Surface-modified hydroxyapatite linked by L-lactic acid oligomer in the absence of catalyst. *Journal of Polymer Science Part A: Polymer Chemistry* 43(21): 51-52.

Raguraman, M. & Rajan, M. 2023. Nanoengineering/ technology for tissue engineering and organ printing. In *Emerging Nanotechnologies for Medical Applications,* edited by Ahmad, N. & Packirisamy, G. Elsevier. pp. 35-54.

Sania, B., Benavente, J., Berg, R.W., Stibius, K., Larsen, M.S., Bohr, H. & Hélix-Nielsen, C. 2012. Tailoring properties of biocompatible PEG-DMA hydrogels with UV light. *Materials Sciences and Applications* 3(6): 425-431.

Soballe, K. & Overgaard, S. 1996. The current status of hydroyapatite coating of prosthesis. *The Journal of Bone & Joint Surgery* 78B: 689-691.

Venkatesan, J., Qian, Z.J., Ryu, B., Thomas, N.V. & Kim, S.K. 2012. Chitosan-amylopectin/hydroxyapatite and chitosan-chondroitin sulfate/hydroxyapatite composite scaffolds for bone tissue engineering, *International Journal of Biological Macromolecules* 51(5): 1033-1042.

Yang, F., Williams, C.G., Wang, D.A., Lee, H. & Manson, P.N. 2005. The effect of incorporating RGD adhesive peptide in polyethylene glycol diacrylate hydrogel on osteogenesis of bone marrow stromal cells. *Biomaterials* 26(30): 5991-5998.

Zhou, Z., Yang, D., Nie, J., Ren, Y. & Cui, F. 2009. Injectable poly (ethylene glycol) dimethacrylate-based hydrogels with hydroxyapatite. *Journal of Bioactive and Compatible Polymers* 24(5): 405-423.

*Corresponding author; email: naeem@kust.edu.pk